SAND2007-0924C

Exploring membrane protein dynamics by multicolor single quantum dot imaging using wide field, TIRF, and hyperspectral microscopy

Diane S. Lidke[*a], Nicholas L. Andrews[a], Janet R. Pfeiffer[a], Howland D.T. Jones[b], Michael B. Sinclair[b], David M. Haaland[b], Alan R. Burns[b], Bridget S. Wilson[a], Janet M. Oliver[a], and Keith A. Lidke[†b]

[a]University of New Mexico, Department of Pathology, Albuquerque, New Mexico 87131;
[b]Sandia National Laboratories, Albuquerque, New Mexico 87185

ABSTRACT

The development of colloidal quantum dots (QDs) for biological imaging has brought a new level of sensitivity to live cell imaging. Single particle tracking (SPT) techniques in particular benefit from the superior photostability, high extinction coefficient and distinct emission spectra of QDs. Here we describe the use of QDs for SPT to study the dynamics of membrane proteins in living cells. We work with the RBL-2H3 mast cell model that signals through the high affinity IgE receptor, FcεRI. Using wide field or Total Internal Reflection Fluorescence (TIRF) microscopy we have achieved simultaneous imaging of two spectrally distinct QDs with frame rates of up to 750 frames/s and localization accuracy of ~10 nm. We also describe the imaging and analysis of QDs using a novel hyperspectral microscope and multivariate curve resolution analysis for multi-color QD tracking. The same QD-tag used for SPT is used to localize proteins at <10 nm resolution by electron microscopy (EM) on fixed membrane sheets.

Keywords: Quantum Dots, Single Particle Tracking, IgE, FcεRI, TIRF, Hyperspectral, Electron Microscopy

1. INTRODUCTION

High resolution bio-imaging techniques, such as single particle tracking (SPT), are powerful tools for monitoring protein dynamics[1]. SPT provides the spatial and temporal resolution necessary to elucidate the motion of single molecules in living cells. Traditionally, SPT studies have employed large, multivalent gold labels that may perturb protein motion or organic fluorophores that suffer from rapid photobleaching. Recently, semiconducting nanocrystals (quantum dots, QDs) have been exploited for SPT[2, 3]. QDs present many advantages for SPT, including their relatively small size (5-30 nm diameter) compared to colloidal gold (>40 nm diameter) and their large extinction coefficients and robust photostability compared to organic fluorophores. These properties allow single molecules to be imaged over long time periods with a minimum of interference from the probe itself. Additionally, the broad absorption and narrow emission spectra of QDs open new avenues for investigation through the ability to simultaneously track multiple proteins of interest tagged with spectrally distinct QDs.

We have used QD-tags to characterize the motion and distribution of the high affinity IgE receptor, FcεRI, on mast cells. FcεRI is a tetrameric ($\alpha\beta\gamma_2$) receptor found on the surface of mast cells and basophils. FcεRI binds IgE with high affinity[4]. The subsequent crosslinking of FcεRI by multivalent antigen activates a tyrosine kinase-mediated signaling cascade leading to the release of histamine and other inflammatory mediators by degranulation. To study FcεRI dynamics, we generated a QD-labeled IgE (QD-IgE) using a biotinylated IgE and streptavidin-conjugated QD. This system provided flexibility in labeling ratios as well as selection of QD color. To avoid crosslinking of receptors by a multivalent probe, it was necessary to ensure that the QD-IgE was monovalent. We have determined that QD-IgE acts as a monovalent reagent inasmuch as it does not crosslink receptors, which would be detected by internalization or degranulation assays (N.L. Andrews *et. al*, in preparation).

[*]dlidke@salud.unm.edu; phone 1 505 272-8375; fax 1 505 272-1435; cellpath.health.unm.edu

†Present address, University of New Mexico, Department of Physics

2. MATERIALS AND METHODS

2.1 Reagents and cell culture

Mouse monoclonal anti-DNP IgE was prepared as previously described[5].

Synthesis and characterization of monovalent QD-IgE will be described in detail elsewhere (N.L. Andrews *et. al*, in preparation). In brief, the FluoReporter® Mini-Biotin-XX Protein Labeling Kit (Molecular Probes) protocol was modified to conjugate biotin-succinimidyl ester to IgE such that the resulting biotin:IgE ratio was <1. Biotin-IgE was then combined in 1:1 stoichiometry with Qdot® Streptavidin conjugate (Molecular Probes, Invitrogen) in phosphate buffered saline (PBS) + 1% bovine serum albumin (BSA) to generate 20 nM stock solutions of monovalent QD-IgE.

RBL-2H3 cells, which constitutively express FcεRI, were grown as a monolayer in 8-well Lab-Tek chambers (Nunc) or on glass coverslips. Cells were labeled with 50 pM QD-IgE for 10 min at 37 °C, and washed with Hanks' buffered saline. For two-color experiments, cells were incubated with a mixture of 50 pM QD655-IgE and 50 pM QD585-IgE.

2.2 Fluorescence Microscopy

Wide field imaging for single particle tracking was performed using an Olympus IX71 inverted microscope equipped with a 100× oil objective (N.A. = 1.4). Excitation was provided by a mercury lamp with a 436 nm BP excitation filter (Chroma). Emission was collected by an Andor iXon electron multiplying CCD (emCCD) camera. The back-projected CCD pixel size was 160 nm and images were acquired at 30 frames/s. For simultaneous imaging of two colors, an OptoSplit II (Cairn Research) image splitter equipped with a 600 nm dichroic mirror, QD585 nm and QD655 nm BP emission filters (Chroma) was used. Typically, a region of interest of 256 × 128 pixels was selected for imaging.

TIRF imaging was performed using an Olympus IX71 inverted microscope equipped with a 60× oil objective (N.A. = 1.45) and back-projected pixel size of 267 nm. Excitation was provided by a 472 nm diode laser (CrystaLaser). For simultaneous imaging of two colors, an OptoSplit II (Cairn Research) image splitter equipped with a 600 nm dichroic mirror, QD565 nm and QD655 nm BP emission filters (Chroma) was used. For frame rates of 500 frames/s or faster, a smaller (256 × 24) region was selected.

All live cell imaging was performed at 35 °C. Temperature was regulated by an objective heater (Bioscience Tools).

Hyperspectral imaging was performed using the system described by Sinclair *et. al*[6]. Hyperspectral confocal fluorescence images from 490 to 800 nm were obtained using a 60× oil objective, 120 nm lateral sampling step size and 240 μs/pixel integration time. 30 pM QDs in PBS were incubated on coverslips for 10 min, rinsed with water and mounted in water for imaging. Under these conditions, individual QDs were observed in the hyperspectral images. QDs were excited using a solid state 488 nm laser (Coherent, Inc.). Images were acquired at room temperature.

2.3 Single QD Tracking

Analysis of the acquired image series was performed as described previously[7] and similar to the method of[2]. Images were processed using DIPImage (Delft University of Technology) and tracking routines were written in MATLAB (The MathWorks, Inc.) that calculate the center of intensity in a region around the maximum at each time step. The intermittent QD fluorescence, or blinking, is accounted for explicitly by these algorithms. From these trajectories, the mean square displacement (MSD) as a function of time interval (Δt) was calculated. The resulting MSD plot is fit to the equation for free diffusion[8]: $MSD = offset + 4D\Delta t$, where *MSD* is the mean square displacement, *D* is the diffusion coefficient, Δt is the time interval, and *offset* is related to the localization accuracy[9]. While other modes of motion were also observed for these proteins, we report only the value for the diffusion coefficient ($D_{1\text{-}3}$) in this discussion, where $D_{1\text{-}3}$ is calculated by fitting the free diffusion equation to the first three points. Localization accuracy of the system was determined by imaging QDs bound to the coverslip for 1,000 frames with 20 ms exposure at 30 frames per second, which yielded accurate localization of the particle center of mass to within 12 nm.

2.4 Electron Microscopy

RBL-2H3 cells were labeled with 30 nM QD-IgE at 37 °C for 30 min. The cells were then fixed in 0.5% PFA for 7 min and membrane sheets were prepared as described in Wilson *et. al*[10]. EM images were acquired using a Hitachi 600 transmission electron microscope.

3. RESULTS

3.1 Wide field SPT

Using a wide field microscope equipped with a sensitive emCCD camera, we tracked individual QDs at video rate with ~10 nm accuracy[11, 12]. Due to the photostability of QDs, we were able to track individual receptors for times much longer (minutes) than possible using organic fluorophores (seconds), as first described by Dahan *et. al*[2]. SPT of QD-IgE bound to the surface of living RBL cells revealed four modes of diffusion behavior, similar to reports of other membrane protein motion using organic fluorophores or gold particles[13]. Specifically we observed free, restricted, directed, and immobilized diffusion. Figure 1A shows sample trajectories of these types of motion. The average diffusion coefficient, $D_{1\text{-}3}$, calculated for the FcεRI receptor was 0.11 ± 0.06 $\mu m^2/s$ (see Figure 1B). We observed that QD-IgE-FcεRI complexes often occupy the same small domains for extended times. Using an image splitter allowed the simultaneous tracking of two spectrally distinct QDs. The use of two colors enabled the localization of two QDs even when they overlapped (see Figure 1C). The movement of receptors was not correlated with each other, suggesting the influence of membrane domains on the receptor proximity rather than homotypic interactions.

In SPT, every molecule is detected and its motion quantified. Therefore, we wanted to determine the contribution of nonspecific binding to our measurements. 50 pM QD-IgE and 50 pM QDs were simultaneously incubated with RBL cells for 10 min at 35 °C. While the majority of cells did not have unlabeled QDs bound to the surface, it was possible to

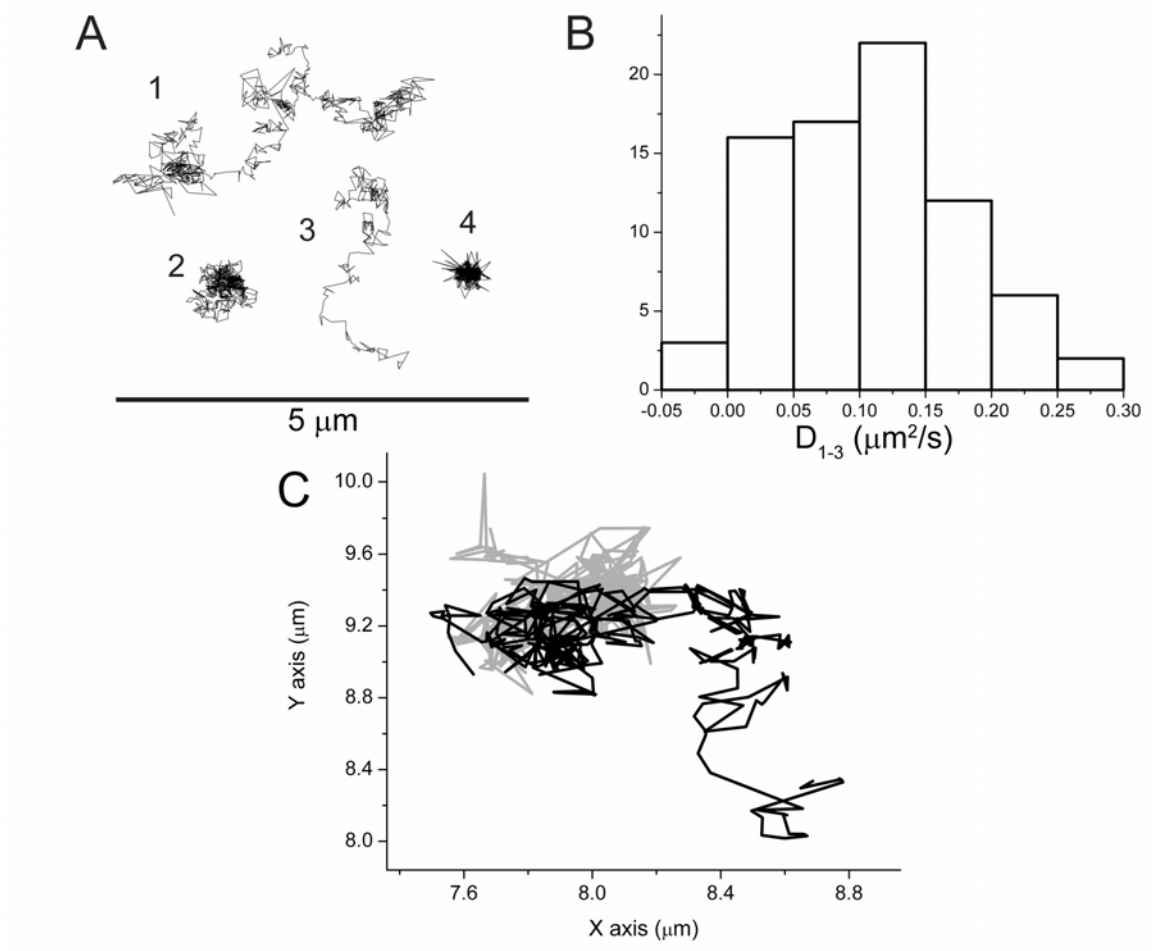

Figure 1. SPT of QD-IgE. A) Sample trajectories of various QD-IgE-FcεRI modes of motion: Free diffusion (1), restricted diffusion (2), directed diffusion (3), and immobile (4). Scale bar is 5 μm. B) Histogram of diffusion coefficients ($D_{1\text{-}3}$) calculated from individual trajectories. C) Overlay trajectories of two QD-IgE-FcεRI complexes (QD655 in black and QD585 in grey) tracked simultaneously.

find some examples of nonspecific binding (Figure 2). The ratio of nonspecific to specific binding (investigating both mixtures of QD655-IgE + QD585 and QD585-IgE + QD655 to avoid possible QD class type dependencies) was 5 QD to 106 QD-IgE (0.047), indicating that < 5% of the particles tracked are nonspecifically bound. We take this to be an upper limit of nonspecific labeling since the presence of IgE that binds with such high affinity to FcεRI may dominate over nonspecific binding events. Under our conditions, QD-IgE was generated using a 1:1 stoichiometry. Based on a Poisson distribution of IgE binding to QDs, we are left with ~37% of the QDs unlabeled. Assuming that the QD-IgE binding is dominated by the IgE interaction, only the unlabeled QDs will bind nonspecifically, resulting in < 2% (0.37*0.047) of the observed binding events. SPT tracking of nonspecifically bound QDs was difficult due to the low level. In the measured trajectories we found that a significant amount (30%) of nonspecifically bound QDs appeared immobile but exhibited a large and sudden shift during the time series that is uncharacteristic of typical QD-IgE motion. One could eliminate trajectories with this type of motion from the analysis, reducing further the small contribution of nonspecific binding.

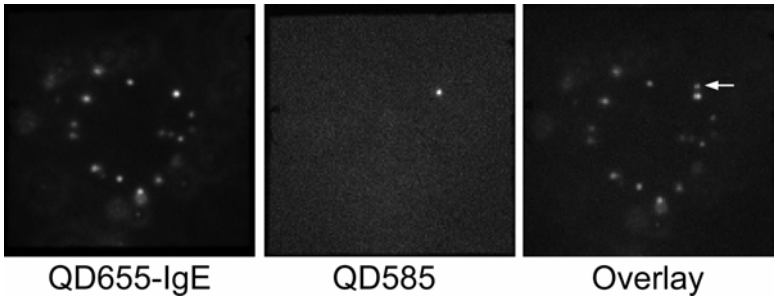

Figure 2. Demonstration of nonspecific binding to living cells. Image of apical surface of RBL-2H3 cells that have been incubated with a mixture of 50 pM QD655-IgE and 50 pM QD585. QD-IgE (left) binds with much higher frequency than unlabeled QDs (middle). Right panel is an overlay with the single QD585 indicated by the arrow. Images are 20 × 20 μm.

3.2 TIRF SPT

In TIRF microscopy, the excitation beam is incident on the coverslip at an angle such that the beam is reflected and only the evanescent wave enters the sample, effectively exciting only molecules close to the surface (~100 nm) and eliminating the background due to out of focus fluorophores[15, 16]. In addition, the excitation intensity of the evanescent wave can be several fold higher than that of the incident light[16], a benefit that is readily taken advantage of since QDs do not suffer from photobleaching. The reduction in background and increase in excitation of TIRF provides a significant improvement in signal-to-noise over conventional wide field microscopy. Imaging in TIRF mode, using the same microscope and detection system as for wide field imaging, we were able to acquire good signal-to-noise images at 750 frames/s using QD655. With the 565 nm emitting QDs, which are less bright, it was possible to image at a frame rate of 500 frames/s. At these rates the $D_{1\text{-}3}$ was found to be 0.19 ± 0.1 $\mu m^2/s$. This result is close to the value of 0.2 $\mu m^2/s$ determined by FRAP of IgE on cells swollen by hypoosmotic stress[17]. This indicates that the use of QDs and sensitive emCCD detection allows us to approach the regime where diffusion in the lipid membrane is unhindered by the cytoskeleton.

The benefits of TIRF microscopy were also exploited to directly observe the interactions of membrane proteins with the actin cytoskeleton (K.A. Lidke *et. al*, in preparation). Simultaneous imaging of the actin cytoskeleton (labeled by GFP-actin) at the basal membrane and QD-IgE-FcεRI complexes demonstrates that there is a confinement process associated with the underlying actin structures. (see Figure 3).

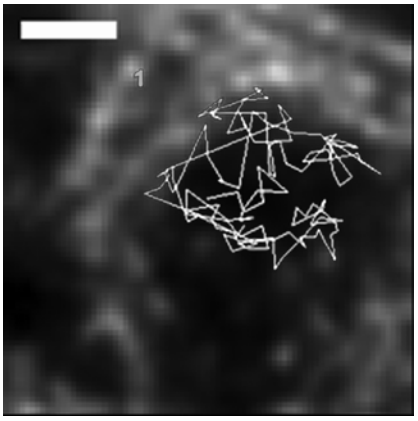

Figure 3. Example of FcεRI confinement by actin. Trajectory of FcεRI over time is shown by the thin white line. Motion is bound by the actin filaments (gray). Scale bar, 1 μm.

3.3 Hyperspectral imaging can distinguish spectrally distinct QDs

Recently, multi-spectral fluorescence imaging (i.e., images with tens of wavelengths measured per sampled point) has become available to improve quantitative accuracy and increase the number of fluorophores that can be monitored. However, the commercial tools (for example, the Zeiss LSM 510 META system) lack, 1) the high spectral resolution necessary for separating highly overlapping emission species, 2) the multivariate analysis methods that are necessary to fully characterize samples in the absence of reference spectra for all emitting species and 3) the speed and sensitivity needed for SPT.

The hyperspectral microscope developed by Sinclair *et. al*[6] is a confocal microscope that captures the entire spectrum for each sampled point and employs an emCCD camera for detection. This microscope can collect >8300 full-emission spectra per second (512 wavelengths in the visible and near-infrared spectral regions, 490 nm to 800 nm) using a proprietary high-throughput imaging prism spectrometer. Multivariate curve resolution (MCR) algorithms[6, 18, 19] can rapidly deconvolve spectra into their different base components, identifying and quantifying all emission sources in a sample without any *a priori* information about emitting species. This system makes possible the single particle detection with high time resolution and rigorous spectral separation that is ideally suited for multi-color SPT and difficult to

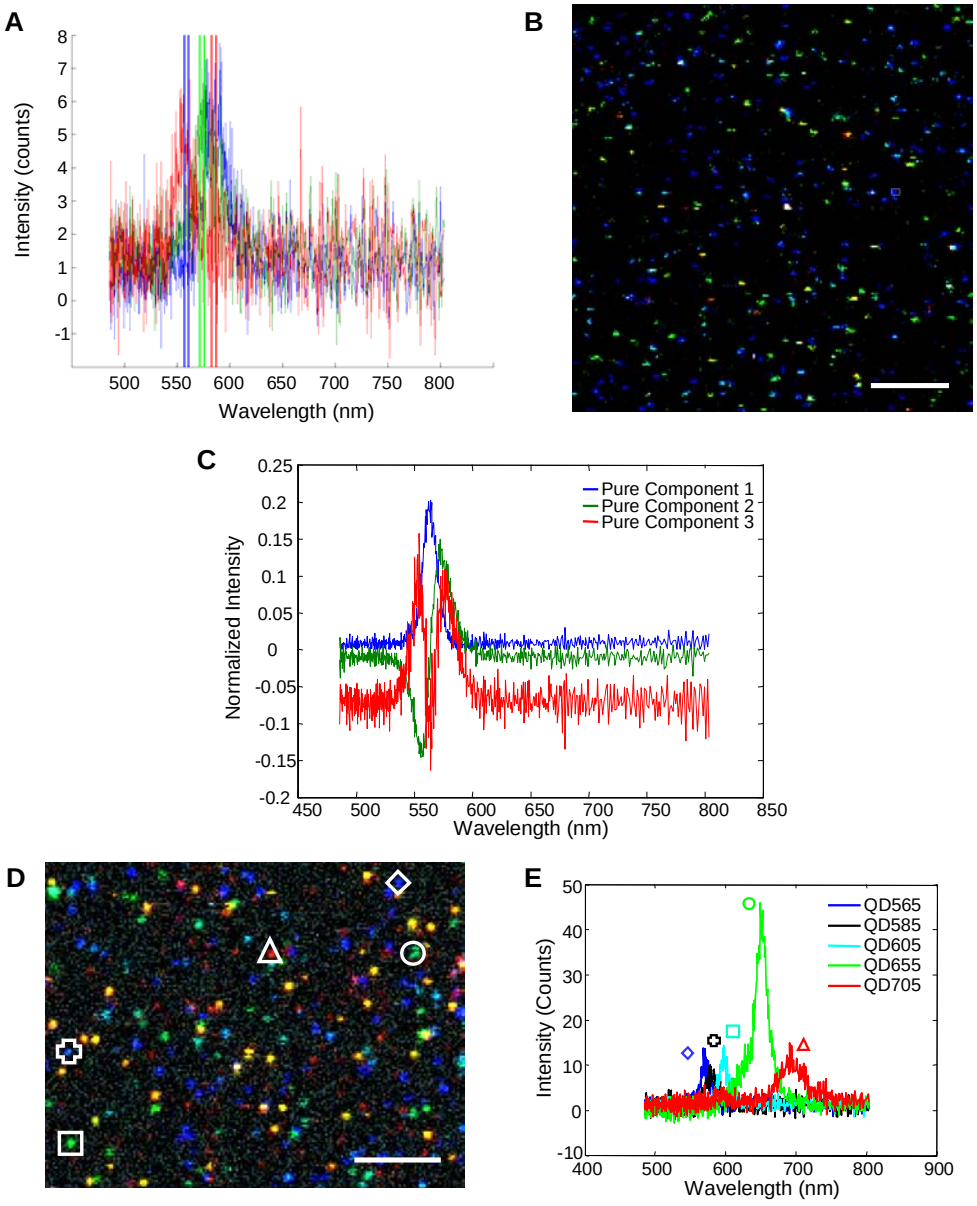

Figure 4. Hyperspectral imaging. A) Examples of individual spectra taken from a sample of 565 nm class of QDs, demonstrating the variation in spectra within a single class of QDs. The color bands indicate integrated regions in computing relative RGB components for Figure B. B) RGB image of 565 nm QDs using filters indicated in A. This is comparable to the image that would be acquired from a three filter system with narrow band pass filters. Scale bar, 5 μm. C) Components used in fitting the spectra data from QD565 sample image (B). D) Image containing a mixture of five spectrally distinct QDs. Scale bar, 5 μm. E) Spectra corresponding to the selected points in D.

achieve in commercial confocal systems.

Hyperspectral images of QDs bound to the coverslip were acquired in order to evaluate the performance of the MCR analysis. The peak emission wavelengths of the ensemble of each class of QDs were as expected; nominally 565, 585, 605, 655, and 705 nm. However, we observed that the spectral position and shape of the individual QDs were variable within a given class of QDs (Figure 4A). An RGB image of the hyperspectral image is presented in Figure 4B. This image was obtained by integrating the signal in the red, green, and blue spectral bands shown in Figure 4A. This observation of spectral variability is assumed to be a result of variations in size and shape of each batch of commercial QDs.

Multivariate curve resolution (MCR), which is a constrained alternating least squares analysis of the hyperspectral images, suggested that each class of QDs could be represented by three independently varying spectral emission components. The MCR analysis was performed with the first component constrained to be non-negative in both the emission spectrum and its concentration. The other two QD spectral components were fully unconstrained. In addition, an offset arising from the emCCD detector was equality constrained during the MCR analysis. Initial starting points for the MCR analysis were the first three principle component analysis (PCA) loading vectors obtained from the hyperspectral images masked just to those pixels containing QDs, and the MCR analysis was performed on the spectra from these same selected pixels. The resulting three pure-emission spectra normalized to unit length are shown in Figure 4C for the 565 nm QDs. These pure-emission spectra can be interpreted as follows: 1) pure-component 1 represents the mean ensemble spectrum of 565 QDs; 2) pure-component 2 is similar to the first derivative of component 1 and represents a shift of the peak emission whose magnitude for a given QD would be related to the peak emission wavelength for the QD; and 3) pure-component 3 is similar to a second derivative of component 1 and represents a narrowing or broadening of the spectral emission for a given QD relative to component 1. Linear combinations of these three pure emissions will represent any given QD in the image to within the noise of the measurement. Similar results were obtained for the 585, 605, and 705 nm classes of QDs. The 655 nm batch of QDs was modeled to within the noise with only two spectral emission components obtained from the MCR analysis of the hyperspectral imaging of these QDs. The two emission components were the average QD emission and the first derivative of this average emission. Apparently, no broadening or narrowing of the QD spectrum was present for this batch of 655 nm QDs.

A mixture of the five classes of QDs was prepared and imaged in the hyperspectral microscope. An RGB image of this sample was generated by integrating the spectral data over three equally spaced bands over the spectral range of 490 to 800 nm (blue, green, and red are represented as the short, middle, and long wavelength bands, respectively) and is presented in Figure 4D with corresponding spectra in Figure 4E. This image represents the image that would be obtained from a three-filter confocal microscope. Figure 4E shows spectra obtained from the individual QDs in the image that represent each of the five classes of QDs in the mixture. Because of the spectral resolution and sensitivity of this hyperspectral microscope, we are actually able to monitor significantly more than five types of QDs because each QD has its own spectral characteristics.

3.4 Electron Microscopy

In addition to the properties that make QDs ideal probes for SPT, they are also electron dense, making them useful for electron microscopy (EM). We obtained EM micrographs of QD-IgE labeled membrane sheets using standard transmission EM. The QD655 appeared as rods on the surface of the sheet (Figure 5). Notice that FcεRI exists in clusters on resting cells, despite the lack of any known homotypic interaction between these receptors. This observation is consistent with previous studies using immunogold labeling[10].

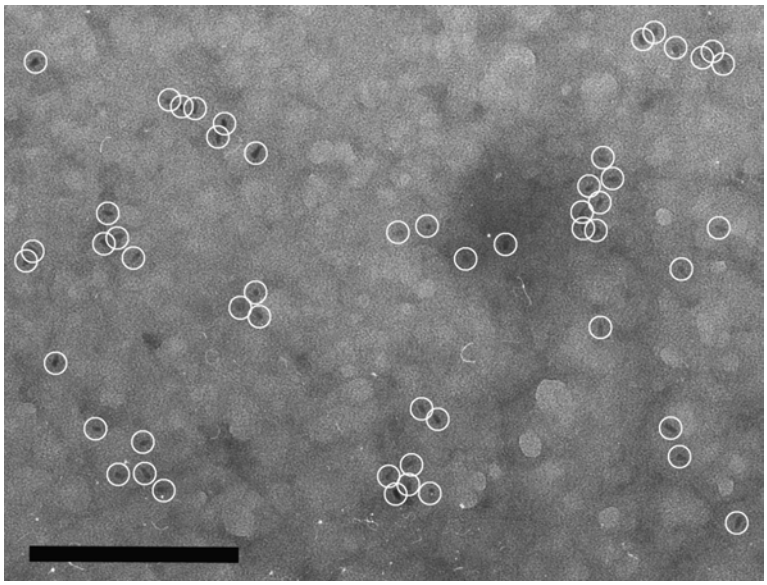

Figure 5 QDs imaged using EM. QD655-IgE bound to the surface of RBL cells. White circles indicate the position of QDs as determined by an automatic particle selection algorithm[20]. Scale bar, 250 nm.

4. DISCUSSION

We have demonstrated the functionality of QDs for single particle imaging using several modes of microscopy. Due to the photostability of QDs one can track molecules for longer times than when using organic fluorophores and take advantage of the enhanced excitation provided in TIRF microscopy. Using TIRF we have imaged individual QDs with a frame rate of 750 frames/s. We have also demonstrated that the same QD-tag used in fluorescence imaging will provide good contrast in EM imaging of membrane sheets due to the electron dense core of the QD. The combined fluorescence and EM imaging properties of QDs allows the same labeling system to be used for direct comparison between the high spatial resolution provided by EM and the dynamic data of SPT.

Combining many spectrally distinct QDs with hyperspectral microscopy presents new opportunities for spectrally multiplexed imaging. We have shown that spectrally distinct QDs can be easily identified within a mixture. Additionally, any particular class of QDs demonstrates variability in spectral position and shape of the individual QD. Since each QD has its own spectral characteristics, we are actually able to monitor significantly more than five types of QDs due to the spectral resolution and sensitivity of this hyperspectral microscope. Development of this technology will be of particular interest for live cell imaging. The hyperspectral microscope described here will make it possible to simultaneously image multiple colors (>3) at high speeds (10 Hz or faster) such that dynamic protein interactions in living cells can be observed.

ACKNOWLEDGEMENTS

This work was supported in part by NIH grants R01 GM49814, R21 EB005365 and P20 GM067594 and by Sandia LDRD and SURP projects. Sandia is a multi-program laboratory operated by Sandia Corporation, a Lockheed Martin Company, for the United States Department of Energy under Contract DE-ACO4-94AL85000. Use of facilities for fluorescence and electron microscopy in the UNM School of Medicine and Cancer Research and Treatment Center is gratefully acknowledged (NCRR 1 S10 RR14668, NSF MCB9982161, NCRR P20 RR11830, NCI P30 CA118100, NCRR S10 RR19287, NCRR S10 RR016918). The particle detection software developed for EM application by J. Zhang and S. Steinberg is available at http://cellpath.health.unm.edu/stmc/emtools/index.html.

REFERENCES

1. D. Marguet, P. F. Lenne, H. Rigneault and H. T. He, "Dynamics in the plasma membrane: how to combine fluidity and order", *Embo J*, **25,** pp.3446-57, 2006.
2. M. Dahan, S. Levi, C. Luccardini, P. Rostaing, B. Riveau and A. Triller, "Diffusion dynamics of glycine receptors revealed by single-quantum dot tracking", *Science*, **302,** pp.442-5, 2003.
3. D. S. Lidke, K. A. Lidke, B. Rieger, T. M. Jovin and D. J. Arndt-Jovin, "Reaching out for signals: filopodia sense EGF and respond by directed retrograde transport of activated receptors", *Journal of Cell Biology*, **170,** pp.619-626, 2005.
4. S. C. Garman, B. A. Wurzburg, S. S. Tarchevskaya, J. P. Kinet and T. S. Jardetzky, "Structure of the Fc fragment of human IgE bound to its high-affinity receptor Fc epsilonRI alpha", *Nature*, **406,** pp.259-66, 2000.
5. F. T. Liu, J. W. Bohn, E. L. Ferry, H. Yamamoto, C. A. Molinaro, L. A. Sherman, N. R. Klinman and D. H. Katz, "Monoclonal dinitrophenyl-specific murine IgE antibody: preparation, isolation, and characterization", *J Immunol*, **124,** pp.2728-37, 1980.
6. M. B. Sinclair, J. A. Timlin, D. M. Haaland and M. Werner-Washburne, "Design, construction, characterization, and application of a hyperspectral microarray scanner", *Applied Optics*, **43,** pp.2079-2088, 2004.
7. D. S. Lidke, K. A. Lidke, B. Rieger, T. M. Jovin and D. J. Arndt-Jovin, "Reaching out for signals: filopodia sense EGF and respond by directed retrograde transport of activated receptors", *J Cell Biol*, **170,** pp.619-26, 2005.
8. D. F. Kucik, E. L. Elson and M. P. Sheetz, "Forward transport of glycoproteins on leading lamellipodia in locomoting cells", *Nature*, **340,** pp.315-7, 1989.
9. D. S. Martin, M. B. Forstner and J. A. Kas, "Apparent subdiffusion inherent to single particle tracking", *Biophys J*, **83,** pp.2109-17, 2002.
10. B. S. Wilson, J. R. Pfeiffer and J. M. Oliver, "Observing FcepsilonRI signaling from the inside of the mast cell membrane", *Journal of Cell Biology*, **149,** pp.1131-1142, 2000.

11. K. A. Lidke, B. Rieger, T. M. Jovin and R. Heintzmann, "Superresolution by localization of quantum dots using blinking statistics", *Optics Express*, **13,** pp.7052-7062, 2005.
12. R. J. Ober, S. Ram and E. S. Ward, "Localization accuracy in single-molecule microscopy", *Biophys J*, **86,** pp.1185-200, 2004.
13. A. Kusumi, Y. Sako and M. Yamamoto, "Confined lateral diffusion of membrane receptors as studied by single particle tracking (nanovid microscopy). Effects of calcium-induced differentiation in cultured epithelial cells", *Biophys J*, **65,** pp.2021-40, 1993.
14. D. S. Lidke, P. Nagy, R. Heintzmann, D. J. Arndt-Jovin, J. N. Post, H. E. Grecco, E. A. Jares-Erijman and T. M. Jovin, "Quantum dot ligands provide new insights into erbB/HER receptor-mediated signal transduction", *Nature Biotechnology*, **22,** pp.198-203, 2004.
15. D. Axelrod, N. L. Thompson and T. P. Burghardt, "Total internal inflection fluorescent microscopy", *J Microsc*, **129,** pp.19-28, 1983.
16. D. Loerke, B. Preitz, W. Stuhmer and M. Oheim, "Super-resolution measurements with evanescent-wave fluorescence excitation using variable beam incidence", *J Biomed Opt*, **5,** pp.23-30, 2000.
17. J. L. Thomas, T. J. Feder and W. W. Webb, "Effects of protein concentration on IgE receptor mobility in rat basophilic leukemia cell plasma membranes", *Biophys J*, **61,** pp.1402-12, 1992.
18. M. H. Van Benthem, M. R. Keenan and D. M. Haaland, "Application of equality constraints on variables during alternating least squares procedures", *Journal of Chemometrics*, **16,** pp.613-622, 2002.
19. D. M. Haaland, J. A. Timlin, M. B. Sinclair, M. H. Van Benthem, M. J. Martinez, A. D. Aragon and M. Werner-Washburne, "Multivariate curve resolution for hyperspectral image analysis: applications to microarray technology", *In Spectral Imaging: Instrumentation, Applications, and Analysis*, **4959,** pp.55-66, 2003.
20. J. Zhang, K. Leiderman, J. R. Pfeiffer, B. S. Wilson, J. M. Oliver and S. L. Steinberg, "Characterizing the topography of membrane receptors and signaling molecules from spatial patterns obtained using nanometer-scale electron-dense probes and electron microscopy", *Micron*, **37,** pp.14-34, 2006.